A Comprehensive Mixed-Mode Time-Domain Load- and Source-Pull Measurement System

A Comprehensive Mixed-Mode Time-Domain Load- and Source-Pull Measurement System

Valeria Teppati, *Member, IEEE*, Andrea Ferrero, *Senior Member, IEEE*, Marco Garelli, *Member, IEEE*, and Serena Bonino

***Abstract*—We present a novel test set devised for nonlinear balanced device characterization using load-pull techniques. The system is capable of measuring the voltage and current waveforms at the calibration reference planes while independently tuning the device under test (DUT) source and load differential- and common-mode terminations. The test set is designed to address present and future large-signal multiport measurement needs, easing the characterization task while developing new multiport active devices.**

***Index Terms*—Balanced devices, differential load-pull, mixed-mode load-pull, multiport calibration, time-domain waveform.**

I. Introduction

DURING the past years, interest in high-frequency balanced amplifiers has exponentially grown. These devices have advantages for RF integrated circuits, such as balanced low-noise front ends [1], [2] and balanced amplifiers [3], as well as balanced line drivers for high-speed digital transmission [4].

The characterization of these high-frequency devices requires rigorous calibration techniques and a multiport test set.

The solutions presented until now generally use balanced passive tuners, making it very difficult, if not impossible, to independently tune the differential- and common-mode loads [5]–[7].

We propose a novel solution for both balanced load- and source-pull based on the active-load technology. The major advantages are the common- and differential-mode independent tuning and great flexibility in performing harmonic load tuning. Moreover, the test set is able to measure the time-domain waveforms for both modes in real time, i.e., the waveforms are displayed while changing the fundamental or harmonic loads. With this system, the principles of waveform engineering can be verified on balanced devices for the first time [8]–[10].

This paper is focused on the novel hardware solution and also provides some measurement examples. Section II presents the system hardware, whereas Section III details the calibration steps. Measurement results are presented in Section IV, and conclusions are drawn in Section V.

Manuscript received October 9, 2008; revised January 16, 2009. First published September 22, 2009; current version published February 10, 2010. The Associate Editor coordinating the review process for this paper was Dr. Yves Rolain.

The authors are with the Department of Electronics, Politecnico di Torino, 10129 Torino, Italy (e-mail: valeria.teppati@polito.it; andrea.ferrero@polito.it; marco.garelli@katamail.com; marco.garelli@polito.it; serena.bonino@polito.it).

Color versions of one or more of the figures in this paper are available online at http://ieeexplore.ieee.org.

Digital Object Identifier 10.1109/TIM.2009.2025071

II. System Description

The four-port measurement system is shown in Fig. 1. It consists of a four-port vectorial measuring system based on four reflectometers [R1, R2, R3, and R4 in Fig. 1(a)] and a vectorial receiver, which sequentially measures the reflectometers' outputs with an SP8T RF switch [Fig. 1(b)]. The system has two mixed-mode active loads, with one connected to the DUT outputs (ports 3 and 4) and the other connected to the DUT inputs (ports 1 and 2). Each load is able to independently synthesize a common- and a differential-mode reflection coefficient. This is accomplished by splitting the incident common- and differential-mode signals with a 3-dB 180° hybrid, independently processing each mode with two active loops and amplifiers, and, finally, recombining the signals with a second hybrid [11].

The active loops consist of a variable attenuator, a phase shifter, and a yttrium–iron–garnet tuned bandpass filter, which is tuned at the frequency of interest (Fig. 2). The active loads can easily be configured to tune the harmonic reflection coefficients: this requires the use of power splitters and additional active loops tuned to the harmonic frequency, as shown in Fig. 1(a) for loops 3 and 4. The advantage of this solution resides in the perfect independent tuning of the harmonic and fundamental loads. Moreover, the harmonic reflection coefficients can be raised up to near-unity magnitude, simulating any highly reflective termination, which is almost impossible with passive tuners. Closed-loop active load-pull systems could have stability issues, as the loop may auto-oscillate, but these problems are greatly reduced by applying the solutions proposed in [12]–[14]. So far, no instability was observed for the presented mixed-mode version nor on its copy, which was implemented in NXP Semiconductors [15].

Once the system is calibrated, the incident and reflected waves at the DUT ports can be computed in both magnitude and phase [16], [17]. In their simplest form, when reference impedance Z_0 is set to 50 Ω at all ports, the mixed-mode waves are computed from the single-ended waves as [19]

$$a_{D1} = \frac{1}{\sqrt{2}}(a_1 - a_2) \qquad a_{C1} = \frac{1}{\sqrt{2}}(a_1 + a_2) \tag{1}$$

$$b_{D1} = \frac{1}{\sqrt{2}}(b_1 - b_2) \qquad b_{C1} = \frac{1}{\sqrt{2}}(b_1 + b_2) \tag{2}$$

$$a_{D2} = \frac{1}{\sqrt{2}}(a_3 - a_4) \qquad a_{C2} = \frac{1}{\sqrt{2}}(a_3 + a_4) \tag{3}$$

$$b_{D2} = \frac{1}{\sqrt{2}}(b_3 - b_4) \qquad b_{C2} = \frac{1}{\sqrt{2}}(b_3 + b_4) \tag{4}$$

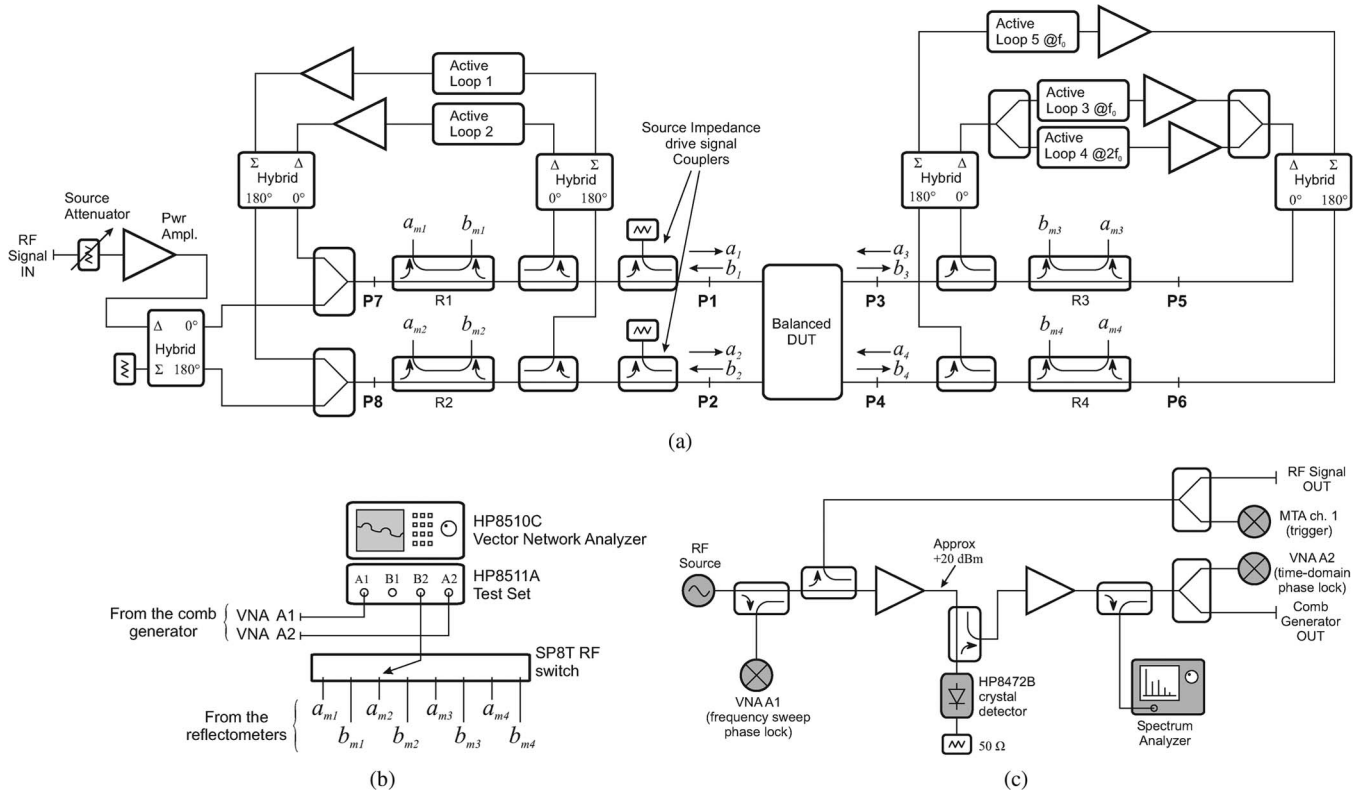

Fig. 1. Novel differential time-domain load-pull system. (a) Main measuring section, including the source and output mixed-mode active loads. The reflectometers' outputs are measured as shown in (b). (b) Detail of the VNA signal paths. The VNA is an HP8510C with an HP8511A test set, which is phase locked on the signals coming from the custom-made comb generator in (c). (c) Custom-made comb generator block schematic. With an RF source frequency of 2 GHz, the useful harmonic content extends up to 10 GHz.

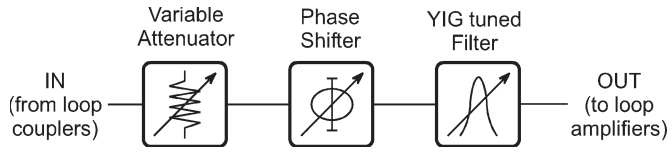

Fig. 2. Active loop configuration.

where b_{D2} and b_{C2} are the differential- and common-mode reflected waves at the DUT outputs, respectively; a_{D2} and a_{C2} are the incident waves; and $(b_{\mathrm{D1}}, a_{\mathrm{D1}})$ and $(b_{\mathrm{C1}}, a_{\mathrm{C1}})$ are the differential- and common-mode waves at the DUT input, respectively.

These definitions set the differential-mode reference impedance $Z_{\mathrm{D}} = 2Z_0 = 100\ \Omega$ and the common-mode reference impedance $Z_{\mathrm{C}} = Z_0/2 = 25\ \Omega$. The general case, where the reference impedances are unequal, is presented in [20], but, in the following, we will adhere to a real single-ended reference impedance $Z_0 = 50\ \Omega$.

Finally, the differential- and common-mode voltages and currents at the reference planes are computed as

$$V_{\mathrm{D1}} = \sqrt{Z_{\mathrm{D}}}[a_{\mathrm{D1}} + b_{\mathrm{D1}}] \qquad I_{\mathrm{D1}} = \frac{1}{\sqrt{Z_{\mathrm{D}}}}[a_{\mathrm{D1}} - b_{\mathrm{D1}}] \quad (5)$$

$$V_{\mathrm{C1}} = \sqrt{Z_{\mathrm{C}}}[a_{\mathrm{C1}} + b_{\mathrm{C1}}] \qquad I_{\mathrm{C1}} = \frac{1}{\sqrt{Z_{\mathrm{C}}}}[a_{\mathrm{C1}} - b_{\mathrm{C1}}] \quad (6)$$

$$V_{\mathrm{D2}} = \sqrt{Z_{\mathrm{D}}}[a_{\mathrm{D2}} + b_{\mathrm{D2}}] \qquad I_{\mathrm{D2}} = \frac{1}{\sqrt{Z_{\mathrm{D}}}}[a_{\mathrm{D2}} - b_{\mathrm{D2}}] \quad (7)$$

$$V_{\mathrm{C2}} = \sqrt{Z_{\mathrm{C}}}[a_{\mathrm{C2}} + b_{\mathrm{C2}}] \qquad I_{\mathrm{C2}} = \frac{1}{\sqrt{Z_{\mathrm{C}}}}[a_{\mathrm{C2}} - b_{\mathrm{C2}}]. \quad (8)$$

We now define a set of parameters of interest. The differential- and common-mode DUT output powers (at the fundamental or harmonic frequencies) are

$$P_{\mathrm{outD}} \equiv |b_{\mathrm{D2}}|^2 - |a_{\mathrm{D2}}|^2 \quad (9)$$

$$P_{\mathrm{outC}} \equiv |b_{\mathrm{C2}}|^2 - |a_{\mathrm{C2}}|^2 \quad (10)$$

and the DUT input powers are

$$P_{\mathrm{inD}} \equiv |a_{\mathrm{D1}}|^2 - |b_{\mathrm{D1}}|^2 \quad (11)$$

$$P_{\mathrm{inC}} \equiv |a_{\mathrm{C1}}|^2 - |b_{\mathrm{C1}}|^2. \quad (12)$$

whereas the differential- and common-mode load reflection coefficients are defined as

$$\Gamma_{\mathrm{LD}} \equiv \frac{a_{\mathrm{D2}}}{b_{\mathrm{D2}}} \quad (13)$$

$$\Gamma_{\mathrm{LC}} \equiv \frac{a_{\mathrm{C2}}}{b_{\mathrm{C2}}}. \quad (14)$$

Finally, the power gains are given by

$$G_{\mathrm{D}} \equiv \frac{P_{\mathrm{outD}}}{P_{\mathrm{inD}}} \quad (15)$$

$$G_{\mathrm{C}} \equiv \frac{P_{\mathrm{outC}}}{P_{\mathrm{inC}}}. \quad (16)$$

In general, the DUT performances are dependent on Γ_{LD} and Γ_{LC} at the fundamental and harmonics.

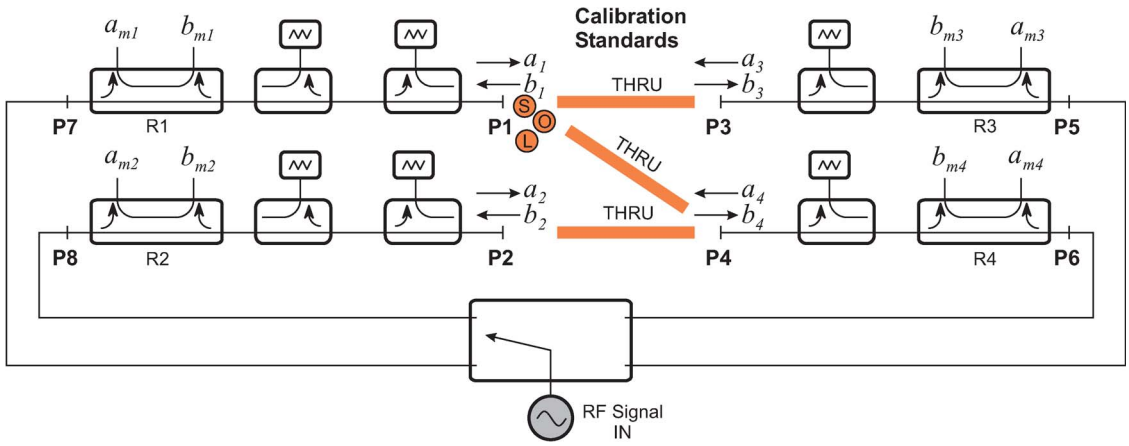

Fig. 3. Example of multiport scattering parameter calibration. Three one-port standards (short–open–load) are used at port 1, and three known thru standards are connected between 1 and 3, 1 and 4, and 2 and 4.

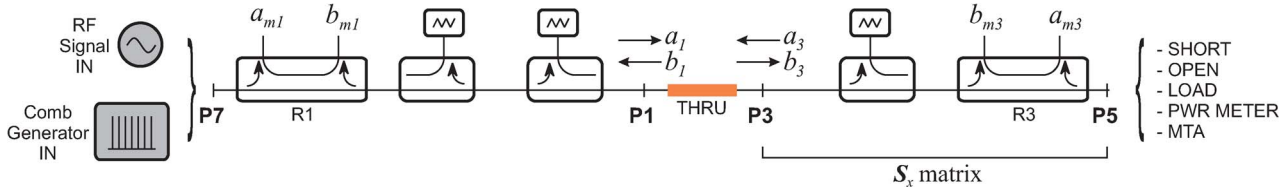

Fig. 4. Power and phase calibration. A thru standard is connected between ports 1 and 3, and short–open–load standards are used at auxiliary port 5.

III. Calibration Model

The measurement system bases its error model on the multiport vector network analyzer (VNA) calibration model [21], [22]. We define a set of error coefficients l_i, m_i, h_i, and k_i for each port i $(i = 1, 2, 3, 4)$

$$\begin{aligned} a_i &= l_i b_{\mathrm{m}i} - h_i a_{\mathrm{m}i} \\ b_i &= k_i b_{\mathrm{m}i} - m_i a_{\mathrm{m}i} \end{aligned} \tag{17}$$

where a_i and $a_{\mathrm{m}i}$ are the actual and measured incident waves at port i, respectively, and b_i and $b_{\mathrm{m}i}$ are the actual and measured reflected waves, respectively (see Fig. 1).

In an n-port VNA without leakage, the scattering error terms are $4n - 1$, with one coefficient being used for normalization. These unknowns need to be computed by a multiport scattering calibration. The calibration problem can be solved by merging together one- and two-port calibrations until all ports are calibrated. A four-port example is shown in Fig. 3, where a quick short–open–load–thru (QSOLT) [23] is performed between ports 1–3; then, the other ports are merged using thru standards. Different multiport calibration schemes can also be employed, and the QSOLT can be substituted by any common two-port calibration type, such as thru–reflect–line, line–reflect–match, short–open–load–thru, or short–open–load–reciprocal.

During the scattering calibration, the drive signal comes from the VNA internal source and is routed by an SP4T switch connected to external ports 5–8. The mixed-mode active loads are disconnected, and the loop couplers are terminated.

The power and phase calibration is based on [24]. This crucial step is needed to compute the normalization error coefficient in magnitude and phase for each frequency. We use a power meter to measure the calibration signal power and a microwave transition analyzer (MTA) to read the harmonic phase information of a comb generator test signal (Fig. 4). Our system uses the calibrated MTA to characterize the harmonic phase content of an uncalibrated comb generator, thus avoiding both the slower MTA readings during the DUT measurement, as in [8], [25], and the transfer standard of any kind for the phase reference, as in [16]–[18]. Thus, the final harmonic phase accuracy for the time-domain waveform measurements is that of the MTA.

The power and phase calibration steps take advantage of an auxiliary port, e.g., port 5, configured to be directly connected to the MTA channel 2 connector; thus, no calibrated adapters are needed to mate the MTA to the measurement ports (1, 2, 3, or 4), which is unpractical in on-wafer applications. A short–open–load calibration is performed at this port, enabling the computation of the $\boldsymbol{S}_x$ scattering matrix of the section from port 3 to port 5, thus including any cables or adapters required to mate the MTA connector [24].

During the power calibration, the power meter is connected to port 5, and the CW signal source at port 7 is set, in turn, at all the calibration frequencies. From the knowledge of $\boldsymbol{S}_x$, the power measurements at port 5 are then translated back to port 3, and the magnitude of the normalization coefficient is computed.

For the phase calibration, as shown in Fig. 4, the MTA is connected to port 5, and the CW source is substituted with the comb generator signal [Fig. 1(c)], which also provides the trigger signal to the MTA and the VNA phase lock, to coherently measure the harmonic signals.

The comb signal is generated by a simple RF detector, which is driven by a strong signal (+20 dBm) at the fundamental frequency [Fig. 1(c)]. The detector's dc output is closed by

a 50-Ω resistor, which provides the dc current return needed to increase the nonlinear effects. A directional coupler then extracts the distorted reflected signal from the detector, and the comb signal is properly amplified. This simple solution showed to be very effective in generating the harmonic reference signals but is not suitable for multitone DUT excitation, such as [26]. The frequency spacing is much larger, but this allows the production of a significant signal up to 10 GHz.

Since the comb generator output is not supposed to vary over time, the MTA information about the harmonic relative phases can be translated to the VNA measurements, and the phase of the normalization coefficient is computed. Therefore, the phase calibration uniquely depends on the MTA accuracy, and the calibration traceability is based on the MTA calibration and not on transfer standards, such as golden diodes. In our case, the MTA is assumed to be calibrated at its input connectors and not to introduce any phase distortion up to 10 GHz.

It is fundamental that the VNA phase locks on the comb generator output; otherwise, the harmonic signals will show random phases. We used an HP8510C VNA coupled with an HP8511A frequency converter. This 20-year-old instrument still remains to be the affordable reference solution for such complex microwave measurements, due to its great flexibility and its analog phase-lock system.

After the calibration, the comb generator output is matched with a 50-Ω load.

IV. Measurement Results

A. Load-Pull Measurements

We measured the performances of an Agilent TC226P balanced amplifier mounted on a connectorized evaluation board. The device is intended for broadband linear operation, but we investigated its behavior close to saturation.

The measurements were performed at 2 GHz, and the harmonic content was measured up to 10 GHz. Fig. 5 shows the results for the fundamental differential-mode load. The device maximum output power is reached slightly off the $Z_{\rm D} = 100\ \Omega$ load condition, and interestingly, the common-mode content drops down when reaching the optimum load condition. This fact is confirmed by the power sweep performed at the optimum load, as shown in Fig. 6. It is worth noting that the common and differential modes of each harmonic frequency are interrelated: One mode has a minimum close to the point of maximum curvature of the other mode. These points differ for each harmonic frequency. To the authors' knowledge, this fact was never reported before.

B. Waveform Measurements

Wave-shaping techniques are heavily used when designing single-ended amplifiers. With balanced devices, the differential-mode performances may be influenced by the common-mode harmonic terminations if enough common-mode output power is present. Even though, if the amplifier is well balanced, it will perform like an equivalent single-ended device for the differential mode.

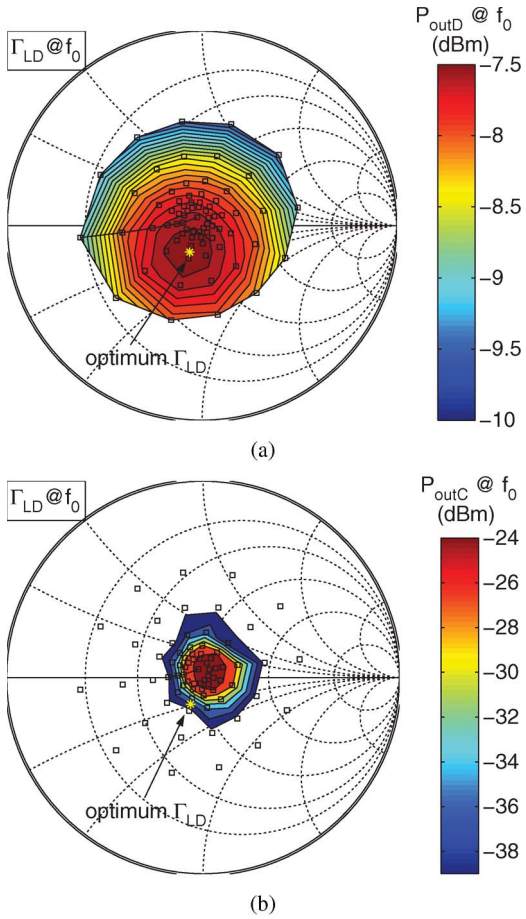

Fig. 5. TC226 differential-mode load map at the fundamental. Shown are the output powers at 1-dB compression of the differential-mode gain. (a) Differential-mode output power versus $\Gamma_{\rm LD}$. (b) Common-mode output power versus $\Gamma_{\rm LD}$.

The time-domain waveforms are computed from the N harmonic phasors as a Fourier series

$$S(t) = \sum_{i=1}^{N} |s_i| \cos(2\pi f_i + \angle s_i) \tag{18}$$

where f_i are the harmonic frequencies, and s_i is the current or voltage phasor of interest, as computed from the respective incident and reflected de-embedded waves.

Fig. 7 shows the wave-shaping results obtained when tuning the second harmonic differential load. In this case, the TC226 device was found to be very well balanced. An additional tuning of the harmonic common-mode loads resulted in no significant changes in the performances. This was also confirmed by analyzing the differential-mode voltage waveform, which showed no effects. The reason is found in Fig. 6: the second harmonic common-mode output power is 10 dB lower than the differential-mode output power.

C. Performance Comparison Between Single-Ended and True Balanced Loads

The mode-tuning independence of the mixed-mode active loads is mostly due to the balance of the 3-dB 180° hybrids.

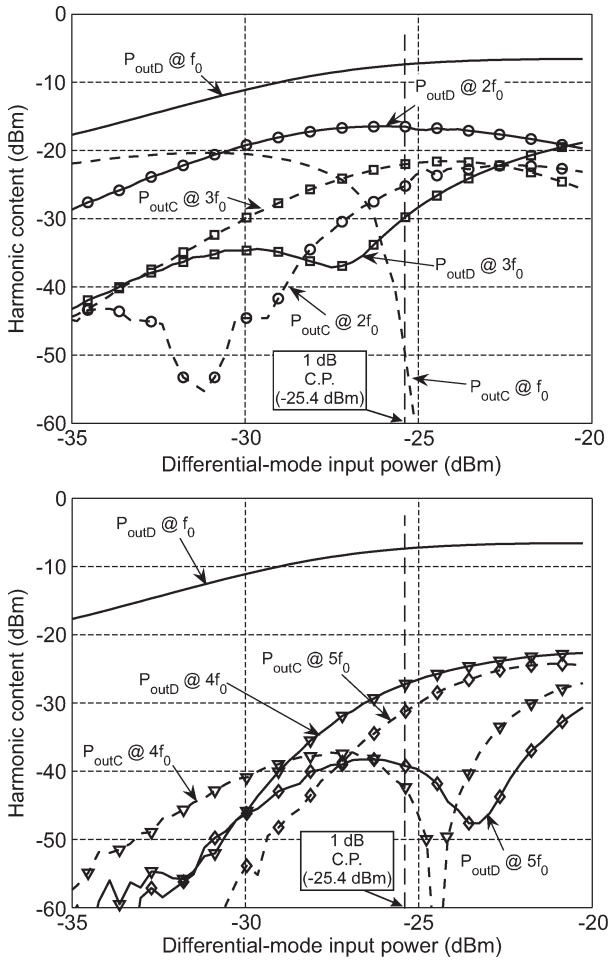

Fig. 6. TC226 differential-mode power sweep at the fundamental. The load is tuned to the optimum differential-mode reflection coefficient. The dashed line indicates the 1-dB compression point.

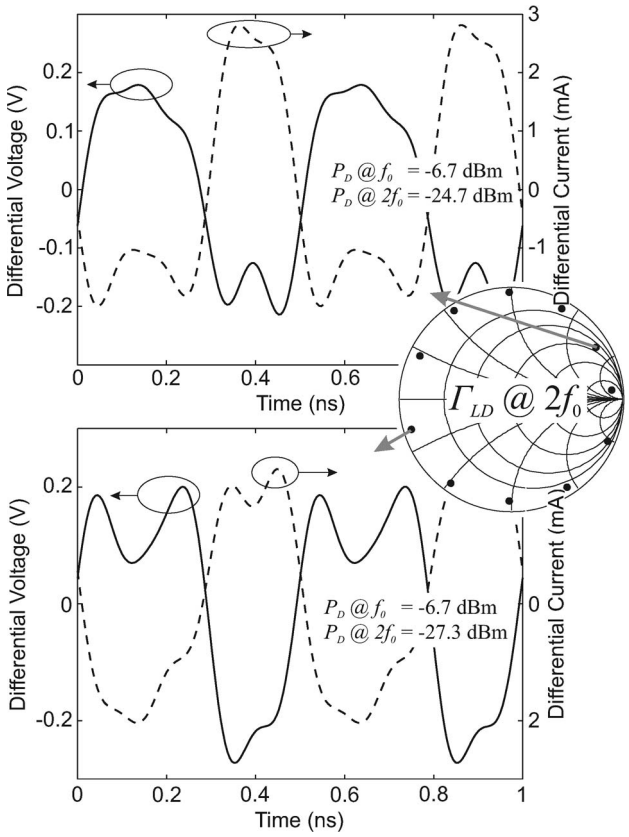

Fig. 7. TC226 differential-mode second harmonic tuning map. The differential load at the fundamental is tuned to the maximum output power point.

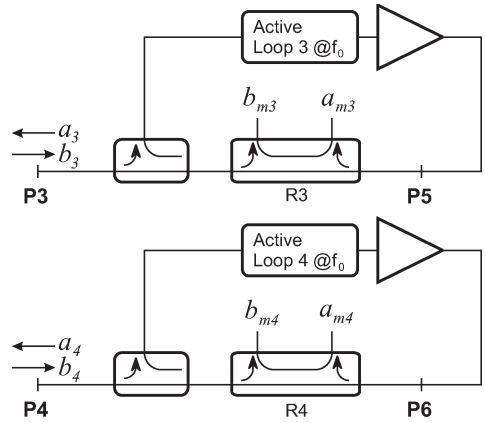

Fig. 8. Experimental configuration with two independent single-ended active loads.

In our implementation, we used 2–18-GHz hybrids, with maximum 5° unbalance and 0.5-dB ripple in the band. Good independence is important in such load-pull measurements and greatly reduces the measurement time.

Anyway, the mixed-mode reflection coefficient independence is not strictly required, as long as both Γ_{LD} and Γ_{LC} can be tuned. The DUT responds to the reflected waves only and is not able to distinguish the source of the reflections, e.g., passive reflection, an externally injected signal, or conversion from the other mode. In the design phase, if the measurement conditions are reproduced by applying the same bias and the same excitation and realizing two independent modal loads equal to the measured Γ_{LD} and Γ_{LC}, the predicted performances will be obtained.

As an example, an AD8351 balanced amplifier mounted on its evaluation board was measured at 2 GHz with the following two different load configurations:

1) mixed-mode load, as shown Fig. 1(a);
2) two-port load made of two independent single-ended active loads (with the hybrids removed, as shown in Fig. 8).

Under both conditions, the fundamental differential- and common-mode load reflection coefficients were tuned to the same values, and the measured DUT performances are reported in Table I. The performances are pretty unchanged in the two cases, and the small differences are due to the imperfect alignment of the two conditions.

TABLE I
PERFORMANCE COMPARISON BETWEEN TWO DIFFERENT LOAD CONFIGURATIONS

Load setting	Γ_{LD} $\lvert\cdot\rvert$	Γ_{LD} $\angle\cdot$	Γ_{LC} $\lvert\cdot\rvert$	Γ_{LC} $\angle\cdot$	P_{outD} (dBm)	P_{outC} (dBm)	G_D (dB)
1) MM	0.67	162°	0.43	118°	-8.0	-18.4	-0.7
2) SE	0.68	162°	0.40	123°	-8.1	-18.1	-0.7

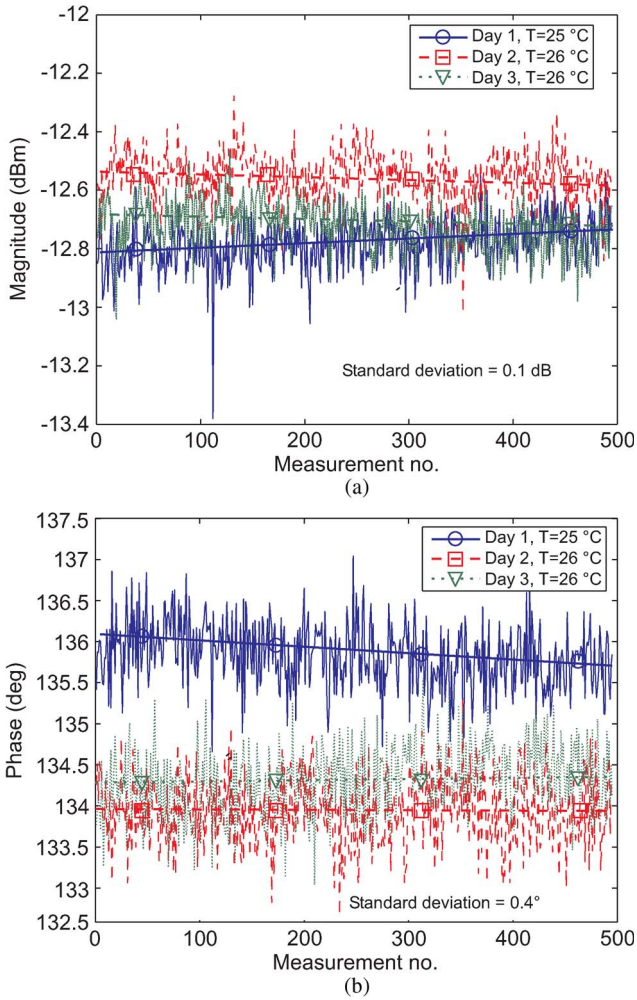

Fig. 9. Comb generator drift measurement for the third harmonic. (a) Magnitude. (b) Phase.

This may suggest the feasibility of using simpler loads, such as two independent passive tuners, but the time required to manually set the load at a particular value would increase. In addition, mixed-mode open-loop active load-pull solutions would carry similar disadvantages since a careful phase synchronization of the synthesized reflected waves to the actual incident waves would be required.

D. Waveform Accuracy Considerations

The repeatability of our comb generator was verified by monitoring its output harmonic content with the MTA. This way, the results are affected by both the comb generator instability and the MTA uncertainty, thus giving an estimate of the overall uncertainty.

Repeated measurements were performed in three consecutive days, with each measurement lasting about 2 h. The purpose was to check for short-term drifts and day-to-day repeatability. The results are plotted in Fig. 9. The harmonic drift was measured up to the fifth component, but the third was found to be the most affected by temperature.

The first trace refers to a small temperature drift, which was achieved by raising the air conditioner temperature from 25 °C to 26 °C. The third harmonic magnitude and phase show measurable dependence on temperature.

The second and third traces refer instead to a steady room temperature and show negligible drifts. In conclusion, the performances are repeatable between two days, and a simple air conditioning system can grant repeatable measurements, provided that the measurement is performed after a warm-up time of about 1 h.

V. Conclusion

A comprehensive test set, which was suitable for mixed-mode time-domain load-pull, has been presented. The closed-loop active-load technique has been found to be crucial in obtaining high reflection coefficient magnitude while preserving the common- and differential-mode tuning independences. This paper has presented a collection of measurement results about high-speed differential amplifiers, showing part of the system capabilities.

A key component for the waveform accuracy is the comb generator. Its drifts have been characterized, and it has been concluded that the generator is repeatable if proper thermal stabilization is provided.

To the author's knowledge, the presented system has unique multiport load-pull capabilities with relatively low cost.

Acknowledgment

The authors would like to thank Y. Rolain and W. Van Moer for providing the balanced devices and helpful discussions, and I. Volokhine for the help and feedback during the measurement system realization.

References

[1] J. Jussila and P. Sivonen, "A 1.2-V highly linear balanced noise-cancelling LNA in 0.13-μm CMOS," *IEEE J. Solid-State Circuits*, vol. 43, no. 3, pp. 579–587, Mar. 2008.

[2] A. M. Ismail and H. Olsson, "A wideband active-feedback low-noise converter for multiband high-linearity low-IF wireless receivers," in *Proc. Bipolar/BiCMOS Circuits Technol. Meeting*, Minneapolis, MN, 2001, pp. 131–134.

[3] M. P. van der Heijden, D. M. H. Hartskeerl, I. Volokhine, V. Teppati, and A. Ferrero, "Large-signal characterization of an 870 MHz inverse class-f cross-coupled push–pull PA using active mixed-mode load-pull," in *Proc. IEEE Radio Frequency Integr. Circuits Symp.*, San Francisco, CA, Jun. 11–13, 2006, p. 392.

[4] D.-H. Han, J.-H. Kim, T. G. Ruttan, and L. A. Polka, "Multi-port measurement-based package model extraction for single-ended and differential signaling," in *Proc. 62nd ARFTG Microw. Meas. Conf.*, Dec. 2003, pp. 1–8.

[5] *Product Catalogue*, Focus Microwaves, Dollard-des-Ormeaux, QC, Canada, 2008.

[6] M. Spirito, M. P. van der Heijden, M. de Kok, and L. C. N. de Vreede, "A calibration procedure for on-wafer differential load-pull measurements," in *Proc. 61st ARFTG Conf.*, Jun. 13, 2003, pp. 1–4.

[7] W. Liu and C. Tsironis, "Load pull characterization system for differential devices," in *Proc. 62nd ARFTG Microw. Meas. Conf.*, Dec. 4–5, 2003, pp. 201–204.

[8] J. Benedikt, R. Gaddi, P. J. Tasker, M. Goss, and M. Zadeh, "High power time domain measurement system with active harmonic load-pull for high efficiency base station amplifier design," in *Proc. IEEE MTT-S Int. Microw. Symp.*, Boston, MA, Jun. 11–16, 2000, vol. 3, pp. 1459–1462.

[9] A. Sheikh, C. Roff, J. Benedikt, P. J. Tasker, B. Noori, P. Aaen, and J. Wood, "Systematic waveform engineering enabling high efficiency

modes of operation in Si LDMOS at both L-band and S-band frequencies," in *Proc. IEEE MTT-S Int. Microw. Symp.*, Atlanta, GA, Jun. 15–20, 2008, pp. 1143–1146.
[10] F. De Groote, J.-P. Teyssier, J. Verspecht, and J. Faraj, "High power on-wafer capabilities of a time domain load-pull setup," in *Proc. IEEE MTT-S Int. Microw. Symp.*, Atlanta, GA, Jun. 15–20, 2008, pp. 100–102.
[11] A. Ferrero and V. Teppati, "A novel active differential/common-mode load for true mixed-mode load-pull systems," in *Proc. IEEE MTT-S Int. Microw. Symp.*, San Francisco, CA, Jun. 2006, pp. 1456–1459.
[12] A. Ferrero, "Active load or source impedance synthesis apparatus for measurement test set of microwave components and systems," U.S. Patent 6 509 743, Jan. 21, 2003.
[13] V. Teppati and A. Ferrero, "A new class of nonuniform, broadband, nonsymmetrical rectangular coaxial-to-microstrip directional couplers for high power applications," *IEEE Microw. Wireless Compon. Lett.*, vol. 13, no. 4, pp. 152–154, Apr. 2003.
[14] V. Teppati, A. Ferrero, and U. Pisani, "Recent advances in real-time load-pull systems," *IEEE Trans. Instrum. Meas.*, vol. 57, no. 11, pp. 2640–2646, Nov. 2008.
[15] I. Volokhine, "Large-signal characterization of balanced power amplifiers," in *Proc. Large-Signal (Sub)mm-Wave Characterization Tech. Symp.,* TU Delft, Oct. 2008, pp. 1–14.
[16] D. Barataud, C. Arnaud, B. Thibaud, M. Campovecchio, J. M. Nebus, and J. P. Villotte, "Measurements of time-domain voltage/current waveforms at RF and microwave frequencies based on the use of a vector network analyzer for characterization of nonlinear devices—Application to high-efficiency power amplifiers and frequency-multipliers optimization," *IEEE Trans. Instrum. Meas.*, vol. IM-47, no. 5, pp. 1259–1264, Oct. 1998.
[17] J. B. Scott, P. S. Blockley, and A. E. Parker, "A new instrument architecture for millimetre-wave time-domain signal analysis," in *Proc. 63rd ARFTG Conf.*, Jun. 2004, pp. 47–52.
[18] I. Volokhine, "An extension of existing real-time load pull systems to perform voltage/current waveform reconstruction," in *Proc. IEEE Microw. Symp.*, Jun. 15–20, 2008, pp. 80–83.
[19] D. E. Bockelman and W. R. Eisenstadt, "Combined differential and common-mode scattering parameters: Theory and simulation," *IEEE Trans. Microw. Theory Tech.*, vol. 43, no. 7, pp. 1530–1539, Jul. 1995.
[20] A. Ferrero and M. Pirola, "Generalized mixed-mode S-parameters," *IEEE Trans. Microw. Theory Tech.*, vol. 54, no. 1, pp. 458–463, Jan. 2006.
[21] A. Ferrero and F. Sanpietro, "A simplified algorithm for leaky network analyzer calibration," *IEEE Microw. Guided Wave Lett.*, vol. 5, no. 4, pp. 119–121, Apr. 1995.
[22] A. Ferrero, V. Teppati, M. Garelli, and A. Neri, "A novel calibration algorithm for a special class of multiport vector network analyzers," *IEEE Trans. Microw. Theory Tech.*, vol. 56, no. 3, pp. 693–699, Mar. 2008.
[23] A. Ferrero and U. Pisani, "QSOLT: A new fast calibration algorithm for two port S parameter measurements," in *Proc. 38th ARFTG Conf.*, San Diego, CA, Dec. 1991, vol. 20, pp. 15–24.
[24] A. Ferrero and U. Pisani, "An improved calibration technique for on-wafer large-signal transistor characterization," *IEEE Trans. Instrum. Meas.*, vol. 42, no. 2, pp. 360–364, Apr. 1993.
[25] A. Ferrero and V. Teppati, "A complete measurement test-set for non-linear device characterization," in *Proc. 58th ARFTG Conf.*, San Diego, CA, Nov. 2001, pp. 101–105.
[26] L. Gomme and Y. Rolain, "A reference signal for a dense frequency grid phase calibration," in *Proc. IEEE Instrum. Meas. Technol. Conf.*, May 12–15, 2008, pp. 49–53.

Valeria Teppati (S'00–M'04) was born in Torino, Italy, on October 20, 1974. She received the Laurea degree in electronic engineering and the Ph.D. degree in electronic instrumentation from the Politecnico di Torino, Torino, in 1999 and 2003, respectively.

In 2003, she joined the Department of Electronics, Politecnico di Torino, as a Research and Teaching Assistant, where she has been an Assistant Professor since 2005. Her research interests include microwave device design, linear and nonlinear measurement design, multiports, calibration, and uncertainty.

Andrea Ferrero (S'86–M'88–SM'06) was born in Novara, Italy, on November 7, 1962. He received the Laurea degree in electronic engineering and the Ph.D. degree in electronics from the Politecnico di Torino, Torino, Italy, in 1987 and 1992, respectively.

In 1988, he was a Microwave Consultant with Aeritalia Company. In 1991, he was a Summer Student with the Microwave Technology Division, Hewlett-Packard, Santa Rosa, CA. In 1995, he was a Guest Researcher with the Department of Electrical Engineering, Ecole Polytechnique de Montréal, Montréal, QC, Canada. He is currently with the Department of Electronics, Politecnico di Torino, where he was an Associate Professor in electronic measurements in 1998 and became a Full Professor in 2006. His research interests are microwave measurement techniques, calibration, and modeling.

Dr. Ferrero was the recipient of the Automatic RF Techniques Group Technology Award for the development and implementation of vector network analyzer calibration algorithms and nonlinear measurement techniques in 2006.

Marco Garelli (S'04–M'09) was born in Cuneo, Italy, in 1981. He received the Laurea Magistrale degree in electronic engineering, in 2005, from the Politecnico di Torino, Torino, Italy, where he is currently working toward the Ph.D. degree in metrology with the Department of Electronics.

In 2007 and 2008, he was a Guest Researcher with the National Institute of Standards and Technology, Boulder, CO, working in the Material and Noise Projects. His research interests include RF and microwave measurement techniques.

Serena Bonino was born in Cuneo, Italy, in 1983. She received the M.S. degree in computer science and electrical engineering from the University of Illinois, Chicago, in 2007 and the Laurea Magistrale degree in electronic engineering, in 2007, from the Politecnico di Torino, Torino, Italy, where she is currently working toward the Ph.D. degree in metrology with the Department of Electronics.

Her research interests include RF and microwave measurement techniques.